SCIENCE CHINA
Information Sciences

• LETTER •

August 2020, Vol. 63 189304:1–189304:3
https://doi.org/10.1007/s11432-019-2641-2

Wald tests for signal detection when uncertainty exists in a target's spatial-temporal steering vector

Weijian LIU, Jingjing LI, Pengxun WANG, Xiufeng ZHA & Yong-Liang WANG*

Wuhan Electronic Information Institute, Wuhan 430019*, China*

Received 23 June 2019/Revised 16 August 2019/Accepted 30 August 2019/Published online 14 May 2020

Citation Liu W J, Li J J, Wang P X, et al. Wald tests for signal detection when uncertainty exists in a target's spatial-temporal steering vector. Sci China Inf Sci, 2020, 63(8): 189304, https://doi.org/10.1007/s11432-019-2641-2

Dear editor,

Multichannel signal detection is a basic problem in signal processing, especially in radar systems [1–3]. In the real world, the signal steering vector is affected by unadjusted array gain-phase error, maneuverable flight, accelerating flight of a target, and other factors that introduce uncertainties [4]. These uncertainties can be largely alleviated in a subspace model. The signal steering vector with uncertainties can be assumed to lie in certain carefully-devised subspaces, but with unknown coordinates [5].

Recently, Ref. [6] investigated the detection problem when uncertainties simultaneously existed in temporal and spatial steering vectors of a target. In this problem, both the spatial and temporal steering vectors were present in certain subspaces with unknown coordinates. This detection problem is referred to as the generalized direction detection in [6], where two adaptive detectors were proposed according to the generalized likelihood ratio test (GLRT). Additionally, Ref. [7] discussed a similar detection problem. While Ref. [6] assumed a homogenous environment, Ref. [7] assumed a partially homogeneous environment and subsequently proposed an adaptive detector based on the two-step GLRT.

Note that no optimum detector exists for the generalized direction detection problem, because coordinates of the signal and noise covariance matrix are unknown. Hence, other detectors can be reasonably designed to improve the detection performance. The widely used Wald test can deliver higher detection performance than the GLRT, e.g., [8]. However, no Wald test has been proposed for the generalized direction detection problem. To address this gap, this study revisits the detection problem in [6], and proposes an adaptive detector for generalized direction detection using the Wald test. In some scenarios, higher detection performance is observed for the proposed Wald test.

Problem formulation. Generalized direction detection can be formulated as the following binary hypothesis [6]:

$$\begin{cases} \mathrm{H}_0 : \boldsymbol{X} = \boldsymbol{N},\ \boldsymbol{X}_L = \boldsymbol{N}_L, \\ \mathrm{H}_1 : \boldsymbol{X} = \boldsymbol{A}\boldsymbol{\theta}\boldsymbol{\alpha}^{\mathrm{H}}\boldsymbol{C} + \boldsymbol{N},\ \boldsymbol{X}_L = \boldsymbol{N}_L, \end{cases} \tag{1}$$

where the $N \times K$ matrix $\boldsymbol{X}$, is the test data matrix; the $N \times L$ matrix $\boldsymbol{X}_L$, is the training data matrix; $\boldsymbol{A}$ is an $N \times J$ full-column-rank matrix; $\boldsymbol{C}$ is an $M \times K$ full-column-rank matrix; $\boldsymbol{\theta}$ is a $J \times 1$ vector; $\boldsymbol{\alpha}$ is an $M \times 1$ vector; $\boldsymbol{N}$ and $\boldsymbol{N}_L$ are noise matrices in the test and training data, respectively. The noise matrices share the same covariance matrix $\boldsymbol{R}$. In (1), $\boldsymbol{A}$ and $\boldsymbol{C}$ are known, while $\boldsymbol{\theta}$, $\boldsymbol{\alpha}$, and $\boldsymbol{R}$ are unknown.

Detector design. We first construct the following $(N^2 + J + M) \times 1$ parameter vector:

$$\boldsymbol{\Theta} = [\boldsymbol{\Theta}_{\mathrm{r}}^{\mathrm{T}}, \boldsymbol{\Theta}_{\mathrm{s}}^{\mathrm{T}}]^{\mathrm{T}} = [\boldsymbol{\theta}^{\mathrm{T}}, \boldsymbol{\alpha}^{\mathrm{T}}, \mathrm{vec}^{\mathrm{T}}(\boldsymbol{R})]^{\mathrm{T}}, \tag{2}$$

where $\boldsymbol{\Theta}_{\mathrm{r}} = \boldsymbol{\theta}$ and $\boldsymbol{\Theta}_{\mathrm{s}} = [\boldsymbol{\alpha}^{\mathrm{T}}, \mathrm{vec}^{\mathrm{T}}(\boldsymbol{R})]^{\mathrm{T}}$. Subsequently, the Wald test is formulated as [9]

$$t_{\mathrm{Wald}} = \hat{\boldsymbol{\Theta}}_{\mathrm{r}_1}^{\mathrm{H}} \{[\boldsymbol{I}^{-1}(\hat{\boldsymbol{\Theta}}_1)]_{\boldsymbol{\Theta}_{\mathrm{r}}, \boldsymbol{\Theta}_{\mathrm{r}}}\}^{-1} \hat{\boldsymbol{\Theta}}_{\mathrm{r}_1}, \tag{3}$$

* Corresponding author (email: ylwangkjld@163.com)

© Science China Press and Springer-Verlag GmbH Germany, part of Springer Nature 2020

where $\hat{\boldsymbol{\Theta}}_{\mathrm{r}_1}$ stands for the maximum likelihood estimation (MLE) of $\boldsymbol{\Theta}_{\mathrm{r}}$ under H_1, and

$$\{[\boldsymbol{I}^{-1}(\boldsymbol{\Theta})]_{\boldsymbol{\Theta}_{\mathrm{r}},\boldsymbol{\Theta}_{\mathrm{r}}}\}^{-1} = \boldsymbol{I}_{\boldsymbol{\Theta}_{\mathrm{r}},\boldsymbol{\Theta}_{\mathrm{r}}}(\boldsymbol{\Theta}) - \boldsymbol{I}_{\boldsymbol{\Theta}_{\mathrm{r}},\boldsymbol{\Theta}_{\mathrm{s}}}(\boldsymbol{\Theta})\boldsymbol{I}^{-1}_{\boldsymbol{\Theta}_{\mathrm{s}},\boldsymbol{\Theta}_{\mathrm{s}}}(\boldsymbol{\Theta})\boldsymbol{I}_{\boldsymbol{\Theta}_{\mathrm{s}},\boldsymbol{\Theta}_{\mathrm{r}}}(\boldsymbol{\Theta}). \quad (4)$$

Moreover,

$$\boldsymbol{I}(\boldsymbol{\Theta}) = \mathrm{E}\left[\left(\frac{\partial \ln f(\boldsymbol{x};\boldsymbol{\Theta})}{\partial \boldsymbol{\Theta}^*}\right)\left(\frac{\partial \ln f(\boldsymbol{x};\boldsymbol{\Theta})}{\partial \boldsymbol{\Theta}^{\mathrm{T}}}\right)\right] \quad (5)$$

is the Fisher information matrix (FIM), where $(\cdot)^*$ denotes conjugate. Eq. (5) is often partitioned into the following block form:

$$\boldsymbol{I}(\boldsymbol{\Theta}) = \mathrm{E}\begin{bmatrix} \boldsymbol{I}_{\boldsymbol{\Theta}_{\mathrm{r}},\boldsymbol{\Theta}_{\mathrm{r}}}(\boldsymbol{\Theta}) & \boldsymbol{I}_{\boldsymbol{\Theta}_{\mathrm{r}},\boldsymbol{\Theta}_{\mathrm{s}}}(\boldsymbol{\Theta}) \\ \boldsymbol{I}_{\boldsymbol{\Theta}_{\mathrm{s}},\boldsymbol{\Theta}_{\mathrm{r}}}(\boldsymbol{\Theta}) & \boldsymbol{I}_{\boldsymbol{\Theta}_{\mathrm{s}},\boldsymbol{\Theta}_{\mathrm{s}}}(\boldsymbol{\Theta}) \end{bmatrix}. \quad (6)$$

Under H_1, the joint probability density function (PDF) of $\boldsymbol{X}$ and $\boldsymbol{X}_L$ is given by

$$f_1(\boldsymbol{X},\boldsymbol{X}_L) = (\pi^N |\boldsymbol{R}|)^{-(K+L)}\mathrm{e}^{-\mathrm{tr}[\boldsymbol{R}^{-1}(\boldsymbol{S}+\boldsymbol{Y}\boldsymbol{Y}^{\mathrm{H}})]}, \quad (7)$$

where $\boldsymbol{Y} = \boldsymbol{X} - \boldsymbol{A}\boldsymbol{\theta}\boldsymbol{\alpha}^{\mathrm{H}}\boldsymbol{C}$ and $\boldsymbol{S} = \boldsymbol{X}_L\boldsymbol{X}_L^{\mathrm{H}}$. Taking the natural logarithm of (7) and then performing the partial derivative with respect to $\boldsymbol{\theta}$ and $\boldsymbol{\theta}^*$, we obtain

$$\partial \ln f_1(\boldsymbol{X},\boldsymbol{X}_L)/\boldsymbol{\theta} = (\boldsymbol{\alpha}^{\mathrm{H}}\boldsymbol{C}\boldsymbol{Y}^{\mathrm{H}}\boldsymbol{R}^{-1}\boldsymbol{A})^{\mathrm{T}}, \quad (8)$$

$$\partial \ln f_1(\boldsymbol{X},\boldsymbol{X}_L)/\boldsymbol{\theta}^* = \boldsymbol{A}^{\mathrm{H}}\boldsymbol{R}^{-1}\boldsymbol{Y}\boldsymbol{C}^{\mathrm{H}}\boldsymbol{\alpha}. \quad (9)$$

After substituting (8) and (9) into (5), we obtain

$$\boldsymbol{I}(\boldsymbol{\theta}) = \mathrm{E}(\boldsymbol{A}^{\mathrm{H}}\boldsymbol{R}^{-1}\boldsymbol{Y}\boldsymbol{C}^{\mathrm{H}}\boldsymbol{\alpha}\boldsymbol{\alpha}^{\mathrm{H}}\boldsymbol{C}\boldsymbol{Y}^{\mathrm{H}}\boldsymbol{R}^{-1}\boldsymbol{A}) = \boldsymbol{\alpha}^{\mathrm{H}}\boldsymbol{C}\boldsymbol{C}^{\mathrm{H}}\boldsymbol{\alpha}\cdot\boldsymbol{A}^{\mathrm{H}}\boldsymbol{R}^{-1}\boldsymbol{A}. \quad (10)$$

$\boldsymbol{I}_{\boldsymbol{\Theta}_{\mathrm{r}},\boldsymbol{\Theta}_{\mathrm{s}}}(\boldsymbol{\Theta})$ and $\boldsymbol{I}_{\boldsymbol{\Theta}_{\mathrm{s}},\boldsymbol{\Theta}_{\mathrm{r}}}(\boldsymbol{\Theta})$ can be verified as zero matrices. Hence, we have

$$\{[\boldsymbol{I}^{-1}(\boldsymbol{\Theta})]_{\boldsymbol{\Theta}_{\mathrm{r}},\boldsymbol{\Theta}_{\mathrm{r}}}\}^{-1} = \boldsymbol{\alpha}^{\mathrm{H}}\boldsymbol{C}\boldsymbol{C}^{\mathrm{H}}\boldsymbol{\alpha}\cdot\boldsymbol{A}^{\mathrm{H}}\boldsymbol{R}^{-1}\boldsymbol{A}. \quad (11)$$

Substituting (11) into (3), we obtain the Wald test for given values of $\boldsymbol{\alpha}$, $\boldsymbol{\theta}$, and $\boldsymbol{R}$:

$$t_{\mathrm{Wald}_{\boldsymbol{\alpha},\boldsymbol{\theta},\boldsymbol{R}}} = \boldsymbol{\alpha}^{\mathrm{H}}\boldsymbol{C}\boldsymbol{C}^{\mathrm{H}}\boldsymbol{\alpha}\cdot\boldsymbol{\theta}^{\mathrm{H}}\boldsymbol{A}^{\mathrm{H}}\boldsymbol{R}^{-1}\boldsymbol{A}\boldsymbol{\theta}. \quad (12)$$

To remove the ambiguity in the MLEs of $\boldsymbol{\theta}$ and $\boldsymbol{\alpha}$ in (7), we impose the constraint $\boldsymbol{\theta}^{\mathrm{H}}\tilde{\boldsymbol{A}}^{\mathrm{H}}\tilde{\boldsymbol{A}}\boldsymbol{\theta} = 1$, where $\tilde{\boldsymbol{A}} = \boldsymbol{S}^{-\frac{1}{2}}\boldsymbol{A}$. Subsequently, the MLE of $\boldsymbol{\theta}$ is [6]

$$\hat{\boldsymbol{\theta}} = \boldsymbol{\theta}_{\max}/(\boldsymbol{\theta}_{\max}^{\mathrm{H}}\tilde{\boldsymbol{A}}^{\mathrm{H}}\tilde{\boldsymbol{A}}\boldsymbol{\theta}_{\max})^{\frac{1}{2}}, \quad (13)$$

where $\boldsymbol{\theta}_{\max}$ is the eigenvector of the matrix

$$\boldsymbol{D}_{\tilde{\boldsymbol{A}},\breve{\boldsymbol{X}}} = [\tilde{\boldsymbol{A}}^{\mathrm{H}}(\boldsymbol{I}_N + \tilde{\boldsymbol{X}}\tilde{\boldsymbol{X}}^{\mathrm{H}})^{-1}\tilde{\boldsymbol{A}}]^{-1}\tilde{\boldsymbol{A}}^{\mathrm{H}}\breve{\boldsymbol{X}}\boldsymbol{P}_{\breve{\boldsymbol{C}}^{\mathrm{H}}}\breve{\boldsymbol{X}}^{\mathrm{H}}\tilde{\boldsymbol{A}}, \quad (14)$$

corresponding to the maximum eigenvalue. In (14), $\tilde{\boldsymbol{X}} = \boldsymbol{S}^{-\frac{1}{2}}\boldsymbol{X}$, $\breve{\boldsymbol{X}} = \tilde{\boldsymbol{X}}(\boldsymbol{I}_K + \tilde{\boldsymbol{X}}^{\mathrm{H}}\tilde{\boldsymbol{X}})^{-\frac{1}{2}}$, $\breve{\boldsymbol{C}} = \boldsymbol{C}(\boldsymbol{I}_K + \tilde{\boldsymbol{X}}^{\mathrm{H}}\tilde{\boldsymbol{X}})^{-\frac{1}{2}}$, and $\boldsymbol{P}_{\breve{\boldsymbol{C}}^{\mathrm{H}}} = \breve{\boldsymbol{C}}^{\mathrm{H}}(\breve{\boldsymbol{C}}\breve{\boldsymbol{C}}^{\mathrm{H}})^{-1}\breve{\boldsymbol{C}}$. Moreover, the MLE of $\boldsymbol{\alpha}$ for a given $\boldsymbol{\theta}$ is [6]

$$\hat{\boldsymbol{\alpha}}_1 = \left[\boldsymbol{C}\left(\boldsymbol{I}_K + \tilde{\boldsymbol{X}}^{\mathrm{H}}\mathbf{P}^{\perp}_{\tilde{\boldsymbol{A}}\boldsymbol{\theta}}\tilde{\boldsymbol{X}}\right)^{-1}\boldsymbol{C}^{\mathrm{H}}\right]^{-1} \cdot \boldsymbol{C}\left(\boldsymbol{I}_K + \tilde{\boldsymbol{X}}^{\mathrm{H}}\boldsymbol{P}^{\perp}_{\tilde{\boldsymbol{A}}\boldsymbol{\theta}}\tilde{\boldsymbol{X}}\right)^{-1}\tilde{\boldsymbol{X}}^{\mathrm{H}}\tilde{\boldsymbol{A}}\boldsymbol{\theta}, \quad (15)$$

where $\boldsymbol{P}^{\perp}_{\tilde{\boldsymbol{A}}\boldsymbol{\theta}} = \boldsymbol{I}_N - \tilde{\boldsymbol{A}}\boldsymbol{\theta}\boldsymbol{\theta}^{\mathrm{H}}\tilde{\boldsymbol{A}}^{\mathrm{H}}/(\boldsymbol{\theta}^{\mathrm{H}}\tilde{\boldsymbol{A}}^{\mathrm{H}}\tilde{\boldsymbol{A}}\boldsymbol{\theta})$. Therefore, substituting (13) into (15), we obtain the final MLE of $\boldsymbol{\theta}$. Moreover, it can be shown that the MLE of $\boldsymbol{R}$ for given values of $\boldsymbol{\theta}$ and $\boldsymbol{\alpha}$ is

$$\hat{\boldsymbol{R}}_1 = \frac{1}{K+L}[\boldsymbol{S} + (\boldsymbol{X} - \boldsymbol{A}\boldsymbol{\theta}\boldsymbol{\alpha}^{\mathrm{H}}\boldsymbol{C})(\boldsymbol{X} - \boldsymbol{A}\boldsymbol{\theta}\boldsymbol{\alpha}^{\mathrm{H}}\boldsymbol{C})^{\mathrm{H}}]. \quad (16)$$

Thus, the MLE of $\boldsymbol{R}$ is obtained by substituting the MLEs of $\boldsymbol{\theta}$ and $\boldsymbol{\alpha}$ into (16). Finally, substituting the MLEs of $\boldsymbol{\alpha}$, $\boldsymbol{\theta}$, and $\boldsymbol{R}$ into (12) yields the final Wald test described as follows:

$$t_{\mathrm{Wald}} = \hat{\boldsymbol{\alpha}}^{\mathrm{H}}\boldsymbol{C}\boldsymbol{C}^{\mathrm{H}}\hat{\boldsymbol{\alpha}}\cdot\hat{\boldsymbol{\theta}}^{\mathrm{H}}\boldsymbol{A}^{\mathrm{H}}\hat{\boldsymbol{R}}_1^{-1}\boldsymbol{A}\hat{\boldsymbol{\theta}}. \quad (17)$$

Eq. (17) takes the form of a signal-to-noise ratio (SNR). Hence, the Wald test in (17) is named the SNR-based generalized direction detector (SNRGDD). Whether the SNRGDD possesses the constant false alarm rate (CFAR) property with respect to the noise covariance matrix is difficult to ascertain by rigorous proof, but can be confirmed in Monte Carlo simulations (see Figure 1).

Numerical examples. The Monte Carlo simulation is used to evaluate the performance of the proposed adaptive detector. The (i,j)th element of $\boldsymbol{R}$ is set to $\boldsymbol{R}(i,j) = \sigma^2\rho^{|i-j|^2}$. The probabilities of detection (PD) and false alarm (PFA) are derived from 10^4 and 100/PFA data realizations, respectively.

When the target's spatial-temporal steering vector contains no uncertainties, the signal component is $\boldsymbol{H} \triangleq \kappa\boldsymbol{a}_0\boldsymbol{b}_0^{\mathrm{H}}$, where κ is the signal amplitude, and $\boldsymbol{a}_0$ and $\boldsymbol{b}_0$ are the actual spatial and temporal steering vectors, respectively. If no uncertainty exists in the target's spatial-temporal steering, the GLRT of the detection problem in (1) (replacing $\boldsymbol{A}\boldsymbol{\theta}\boldsymbol{\alpha}^{\mathrm{H}}\boldsymbol{C}$ with $\kappa\boldsymbol{a}\boldsymbol{b}^{\mathrm{H}}$) can be obtained as [6]

$$t_0 = \frac{\left|\boldsymbol{a}^{\mathrm{H}}\boldsymbol{S}^{-1}\boldsymbol{X}(\boldsymbol{I}_K + \boldsymbol{X}^{\mathrm{H}}\boldsymbol{S}^{-1}\boldsymbol{X})^{-1}\boldsymbol{b}\right|^2}{\boldsymbol{a}^{\mathrm{H}}(\boldsymbol{S}+\boldsymbol{X}\boldsymbol{X}^{\mathrm{H}})^{-1}\boldsymbol{a}\boldsymbol{b}^{\mathrm{H}}(\boldsymbol{I}_K + \boldsymbol{X}^{\mathrm{H}}\boldsymbol{S}^{-1}\boldsymbol{X})^{-1}\boldsymbol{b}}, \quad (18)$$

which is denoted as GLRT_0 for convenience. In (18), $\boldsymbol{a}$ and $\boldsymbol{b}$ are nominal spatial and temporal steering vectors, respectively. These vectors may differ from $\boldsymbol{a}_0$ and $\boldsymbol{b}_0$, which are expressed as follows:

$$\boldsymbol{a}_0 = \dot{\boldsymbol{a}}(\beta_0) \triangleq [1, \mathrm{e}^{\mathrm{j}2\pi\beta_0}, \ldots, \mathrm{e}^{\mathrm{j}2\pi(N-1)\beta_0}]^{\mathrm{T}}, \quad (19)$$

and

$$\boldsymbol{b}_0 = \dot{\boldsymbol{b}}(f_{d_0}) \triangleq [1, \mathrm{e}^{\mathrm{j}2\pi f_{d_0}}, \cdots, \mathrm{e}^{\mathrm{j}2\pi(K-1)f_{d_0}}]^{\mathrm{T}}, \quad (20)$$

where β_0 and f_{d_0} are the normalized spatial frequency and normalized Doppler frequency of the target, respectively. In the GLRT$_0$, $\boldsymbol{a} = \dot{\boldsymbol{a}}(\beta)$ and $\boldsymbol{b} = \dot{\boldsymbol{b}}(f_d)$ share the same forms as (19) and (20), respectively, but with possibly different β and f_d. The SNR is defined as

$$\mathrm{SNR} = |\kappa|^2 \cdot \boldsymbol{b}_0^{\mathrm{H}} \boldsymbol{b}_0 \cdot \boldsymbol{a}_0^{\mathrm{H}} \boldsymbol{R}^{-1} \boldsymbol{a}_0. \quad (21)$$

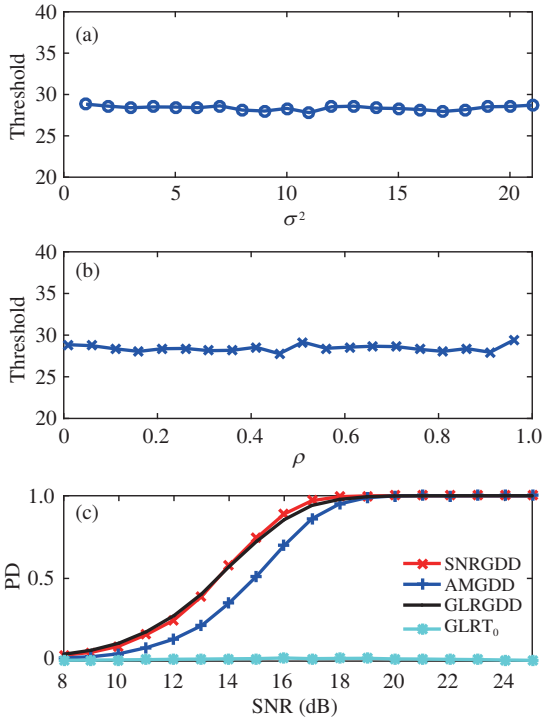

Figure 1 (Color online) Detection performance of the SNRGDD. Detection threshold of the SNRGDD vs. σ^2 (a) and ρ (b). (c) Pds of the detectors. The parameters are PFA $= 10^{-3}$, $L = 2N$, $J = 2$, $M = 2$, $K = 8$, $\boldsymbol{A} = [\dot{\boldsymbol{a}}(0.15), \dot{\boldsymbol{a}}(0.15873)]$, and $\boldsymbol{C} = [\dot{\boldsymbol{b}}(0.34), \dot{\boldsymbol{b}}(0.42)]^{\mathrm{T}}$. In (a), $\rho = 0.95$, in (b), $\sigma^2 = 1$, and in the GLRT$_0$ of (c), $\boldsymbol{a} = \dot{\boldsymbol{a}}(0.15)$ and $\boldsymbol{b} = \dot{\boldsymbol{b}}(0.34)$.

For comparative purposes, the GLR-based generalized direction detector (GLRGDD) and the adaptive matched generalized direction detector (AMGDD) in [6] are also considered. In the SNRGDD, AMGDD, and GLRGDD, the spatial steering matrix $\boldsymbol{A}$ and temporal steering matrix $\boldsymbol{C}$ are formulated as $\boldsymbol{A} = [\boldsymbol{a}_1, \boldsymbol{a}_2, \ldots, \boldsymbol{a}_J]$ and $\boldsymbol{C} = [\boldsymbol{c}_1, \boldsymbol{c}_2, \ldots, \boldsymbol{c}_M]^{\mathrm{T}}$, respectively, where $\boldsymbol{a}_i = \dot{\boldsymbol{a}}(\beta_i)$, $i = 1, 2, \ldots, J$, and $\boldsymbol{c}_i = \dot{\boldsymbol{c}}(f_{d_k})$, $k = 1, 2, \ldots, K$.

Figure 1 shows the detection performance of the SNRGDD. As demonstrated in Figure 1(a) and (b), the detection threshold of the SNRGDD is not dramatically altered by changing σ^2 or ρ, thereby confirming that the SNRGDD has the CFAR property. The plot in Figure 1(c) highlights that when uncertainty exists in both the spatial and temporal steering vectors, the SNRGDD delivers the best detection performance in the PD > 0.6 range followed by the GLRGDD, AMGDD, and GLRT$_0$. The latter method is nearly invalid because its PD is approximately zero.

Acknowledgements This work was supported by National Natural Science Foundation of China (Grant No. 61501505), Natural Science Foundation of Hubei Province (Grant No. 2017CFB589), and National Natural Science Foundation of China and Civil Aviation Administration of China (Grant No. U1733116).

References

1 Hao C P, Gazor S, Foglia G, et al. Persymmetric adaptive detection and range estimation of a small target. IEEE Trans Aerosp Electron Syst, 2015, 51: 2590–2604
2 Liu J, Liu W J, Gao Y C, et al. Persymmetric adaptive detection of subspace signals: algorithms and performance analysis. IEEE Trans Signal Process, 2018, 66: 6124–6136
3 Liu W J, Liu J, Gao Y C, et al. Multichannel signal detection in interference and noise when signal mismatch happens. Signal Process, 2020, 166: 107268
4 Liu J, Zhou S H, Liu W J, et al. Tunable adaptive detection in colocated MIMO radar. IEEE Trans Signal Process, 2018, 66: 1080–1092
5 Yu X X, Cui G L, Kong L J, et al. Constrained waveform design for colocated MIMO radar with uncertain steering matrices. IEEE Trans Aerosp Electron Syst, 2019, 55: 356–370
6 Liu W J, Liu J, Huang L, et al. Robust GLRT approaches to signal detection in the presence of spatial-temporal uncertainty. Signal Process, 2016, 118: 272–284
7 Liu W J, Gao F, Luo Y W, et al. GLRT-based generalized direction detector in partially homogeneous environment. Sci China Inf Sci, 2019, 62: 209303
8 Liu W J, Liu J, Li H, et al. Multichannel signal detection based on wald test in subspace interference and Gaussian noise. IEEE Trans Aerosp Electron Syst, 2019, 55: 1370–1381
9 Liu W J, Wang Y L, Xie W C. Fisher information matrix, Rao test, and Wald test for complex-valued signals and their applications. Signal Process, 2014, 94: 1–5